Journal of
Materials Chemistry A

Materials for energy and sustainability

Accepted Manuscript

This article can be cited before page numbers have been issued, to do this please use: C. Jeffreys, Y. He, N. Alshehri, L. Zhao, A. V. Marsh, G. T. Harrison, O. Matiash, A. Yazmaciyan, C. E. Petoukhoff, S. Fatayer, F. Laquai and M. Heeney, *J. Mater. Chem. A*, 2026, DOI: 10.1039/D6TA01925K.

This is an Accepted Manuscript, which has been through the Royal Society of Chemistry peer review process and has been accepted for publication.

Accepted Manuscripts are published online shortly after acceptance, before technical editing, formatting and proof reading. Using this free service, authors can make their results available to the community, in citable form, before we publish the edited article. We will replace this Accepted Manuscript with the edited and formatted Advance Article as soon as it is available.

You can find more information about Accepted Manuscripts in the Information for Authors.

Please note that technical editing may introduce minor changes to the text and/or graphics, which may alter content. The journal's standard Terms & Conditions and the Ethical guidelines still apply. In no event shall the Royal Society of Chemistry be held responsible for any errors or omissions in this Accepted Manuscript or any consequences arising from the use of any information it contains.

ROYAL SOCIETY OF CHEMISTRY

rsc.li/materials-a

View Article Online
DOI: 10.1039/D6TA01925K

Journal Name ARTICLE

All-Polymer Heterojunction Nanoparticles Enable Reproducible and Enhanced Hydrogen Evolution Photocatalysis

View Article Online
DOI: 10.1039/D6TA01925K

Received 00th January 20xx,
Accepted 00th January 20xx

DOI: 10.1039/x0xx00000x

Charles Jeffreys[a], Yakun He[a], Nisreen Alshehri[a,b], Lingyun Zhao[c], Adam V. Marsh[a], George T. Harrison[a], Oleksandr Matiash[a], Aren Yazmaciyan[a,d], Christopher E. Petoukhoff[a], Shadi Fatayer[a], Frédéric Laquai[a,e], Martin Heeney[a,f]*

Organic semiconducting nanoparticle blends represent a promising platform for renewable photocatalytic hydrogen generation. Their performance strongly depends on microstructure and particle size. Here, we demonstrate the fabrication and characterization of heterojunction nanoparticles made from the donor polymer PM6 and the polymeric acceptor PJ1-R, a polymer analogue of a benchmark small-molecule acceptor Y6. The all-polymer PM6:PJ1-R system exhibited significantly improved photocatalytic performance compared to PM6:Y6 nanoparticles, with an optimal hydrogen evolution rate of 24.89 μmol cm^{-2} h^{-1} in the presence of ascorbic acid as a sacrificial hole scavenger, representing a 2.5-fold increase at optimal blend ratios. Preparation of the all-polymer PM6:PJ1-R nanoparticles was highly reproducible, yielding consistent size distributions (80–120 nm) without aggregation, even after extended storage (12 months), as well as consistent batch-to-batch hydrogen evolution rates. Morphological characterization using transmission electron microscopy revealed beneficial intermixed morphologies with local lamellar ordering, while extensive photophysical analysis (UV-Vis, photoluminescence, time-resolved photoluminescence, and transient absorption spectroscopy) confirmed efficient and complementary charge transfer between PM6 and PJ1-R, with high photoluminescence quenching efficiencies (83.6% for donor, 85.7% for acceptor). These results underline the potential of all-polymer blends in organic semiconductor photocatalysts.

Introduction

Hydrogen is a promising clean energy carrier that has the potential to play an important role in the transition towards a sustainable energy future. Its high energy density, versatility, and the fact that its oxidation produces only water as a by-product make it an appealing alternative to fossil fuels.[1–3] However, roughly 96% of hydrogen production currently relies on fossil fuel-based processes - such as steam methane reforming, naphtha reforming, and coal gasification - all of which contribute to greenhouse gas emissions.[4] As a result, hydrogen arguably offers no clear advantage in reducing CO_2 emissions unless greener production methods are adopted. To establish hydrogen as a truly sustainable energy carrier, requires the development of low-carbon production pathways including methods such as photocatalysis, renewable-energy powered electrolysis, and bio-hydrogen generation. Advancing these technologies is essential for reducing costs, improving efficiency, and enabling large-scale adoption.[1,2,4]

Conventional photocatalysts like titanium dioxide (TiO_2) and graphitic carbon nitride (g-C_3N_4) have been extensively investigated for hydrogen evolution, yet they exhibit limited activity under solar spectrum (AM1.5) illumination. Their relatively large band gap energies (3.2 eV and 2.7 eV, respectively) restrict absorption primarily to ultraviolet (UV) light, which accounts for less than 5% of the solar spectrum.[5–7] Although recent developments in inorganic materials, such as aluminium doped $SrTiO_3$ have achieved impressive efficiencies (96% internal quantum efficiency at 350-360 nm),[8] their performance is fundamentally limited by their predominant UV absorption. Consequently recent efforts have focused on visible-light-driven catalysts to capture a broader portion of the solar spectrum.[5,6] In contrast to the traditional inorganic catalysts, organic semiconducting materials offer tunable optical and electronic properties that can be readily engineered through molecular design. Their narrower band gap energies enable absorbance across the visible region, making them attractive for solar driven photocatalysis.[9,10] Moreover their precise design allows for fine tuning of optoelectronic properties, which are critical to enhancing charge separation, improving light absorption in the visible range, or increasing stability under operational conditions.[11–13]

Despite their potential advantages, organic semiconductor (OSC) materials have relatively low dielectric constants, resulting in high exciton binding energies. To overcome this, efficient charge generation relies on exciton separation at an interface between two complementary semiconductors. This, in turn, requires a large interfacial area, typically accomplished through the formation of a bulk heterojunction (BHJ) containing intermixed donor and acceptor components.[14] High-performing BHJs usually combine polymeric donor materials with small-molecule acceptor (SMA) materials, an architecture that has enabled excellent performance in organic photovoltaic (OPV) devices, with power conversion efficiencies over 20%.[15–19] These improvements stem from the development of non-fullerene acceptors with enhanced light absorption, improved energy level alignment, and optimised morphologies that promote efficient exciton dissociation and charge transport.

[a] Physical Science and Engineering Division, King Abdullah University of Science and Technology (KAUST), Thuwal 23955-6900, Kingdom of Saudi Arabia. E-mail: martin.heeney@kaust.edu.sa
[b] Physics and Astronomy Department, College of Sciences, King Saud University, Riyadh 12372, Kingdom of Saudi Arabia.
[c] KAUST Core Labs, King Abdullah University of Science and Technology (KAUST), Thuwal, Kingdom of Saudi Arabia.
[d] Paul Drude Institute for Solid State Electronics, Hausvogteiplatz 5-7, Berlin 10117, Germany.
[e] Chair of Physical Chemistry and Spectroscopy of Energy Materials, Department of Chemistry, Ludwig-Maximilians-Universität München, Munich 81377, Germany.
[f] Department of Chemistry and Centre for Processable Electronics, Imperial College London, White City Campus, London, W12 0BZ, UK.

View Article Online
DOI: 10.1039/D6TA01925K

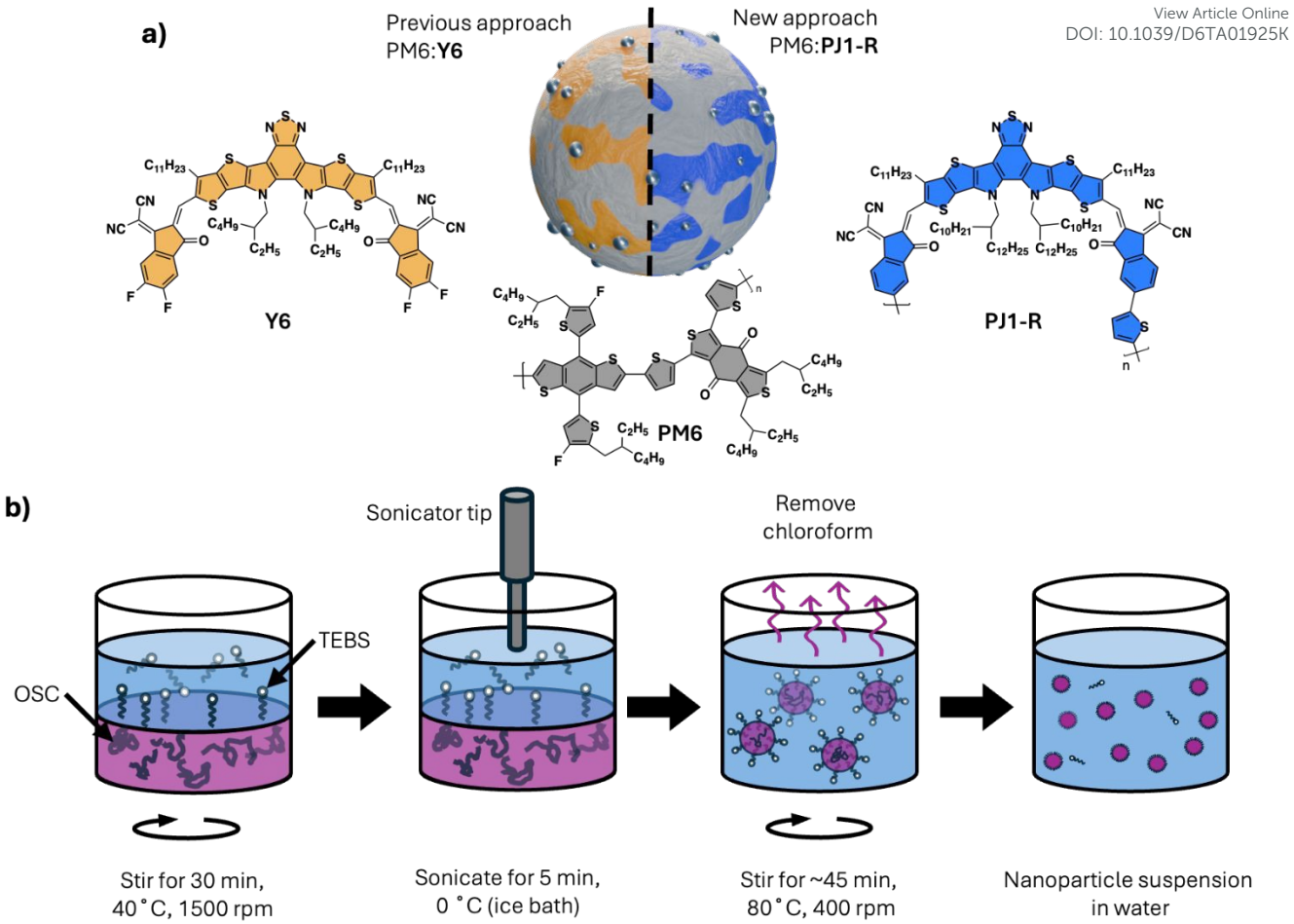

Figure 1. a) Representation of a bulk heterojunction nanoparticle showing the structures of the donor polymer PM6 and the acceptor materials, small molecule Y6 and polymer PJ1-R. b) Schematic representation of nanoparticle fabrication via mini-emulsion method.

The translation of BHJ concepts to photocatalytic systems for hydrogen evolution was reported in 2020 by Kosco et al.,[20] who demonstrated that surfactant-stabilised BHJ nanoparticles prepared by a mini-emulsion technique yielded unprecedented rates of hydrogen evolution from an organic photocatalyst. Subsequent studies have explored diverse donor-acceptor combinations, morphologies, and applications of this technology.[21–26] Whilst development has progressed rapidly, driven by developments in the OPV field, significant challenges remain, not least the reproducibility. For efficient nanoparticle-based hydrogen generation, the deposition of a co-catalyst (typically Pt or Pd) on the nanoparticle surface is required. This is usually performed by photoreduction and occurs selectively on the electron-deficient component of the phase segregated nanoparticle. The deposition is therefore very sensitive to surface microstructure, with variations in nanoparticle size and composition also leading to inconsistent catalytic performance. We believe these issues could be linked to the highly crystalline and strongly aggregating nature of SMA materials. Excessive crystallinity can cause phase segregation and limited polymer–acceptor miscibility, producing heterogeneous nanoparticle populations with poor morphological control. To address this limitation, we propose that replacing the small-molecule acceptor with a polymer acceptor could help to suppress uncontrolled aggregation and improve reproducibility. Polymer acceptors have already demonstrated excellent compatibility and stability in BHJ thin films,[27,28] yet their use in photocatalytic BHJ nanoparticles has been scarcely explored.[29]

A promising alternative to SMAs for nanoparticle applications is polymerised-small-molecule-acceptors (PSMAs). Since 2017, PSMAs have undergone significant investigation and optimisation, and thus have seen application in a range of fields such as OPVs, organic light emitting diodes (OLEDs), organic field-effect transistors (OFETs), and organic photodetectors (OPDs).[30–33] PSMAs have also seen application as single component organic photocatalysts, showing promise in hydrogen evolution reaction (HER) applications.[34–37] However as noted above, single component systems can suffer from poor exciton dissociation and inefficient charge generation. Herein, we demonstrate that integrating a PSMA (i.e., PJ1-R) as the acceptor material in organic nanoparticles for photocatalytic hydrogen evolution under sacrificial conditions results in a 2.5-fold performance increase compared to a SMA analogue, along with significantly improved reproducibility.

Results and Discussion

In selecting our PSMA we focused on a regioregular derivative of the reported polymer PJ1. This PSMA, PJ1-R, eliminates complications

View Article Online
DOI: 10.1039/D6TA01925K

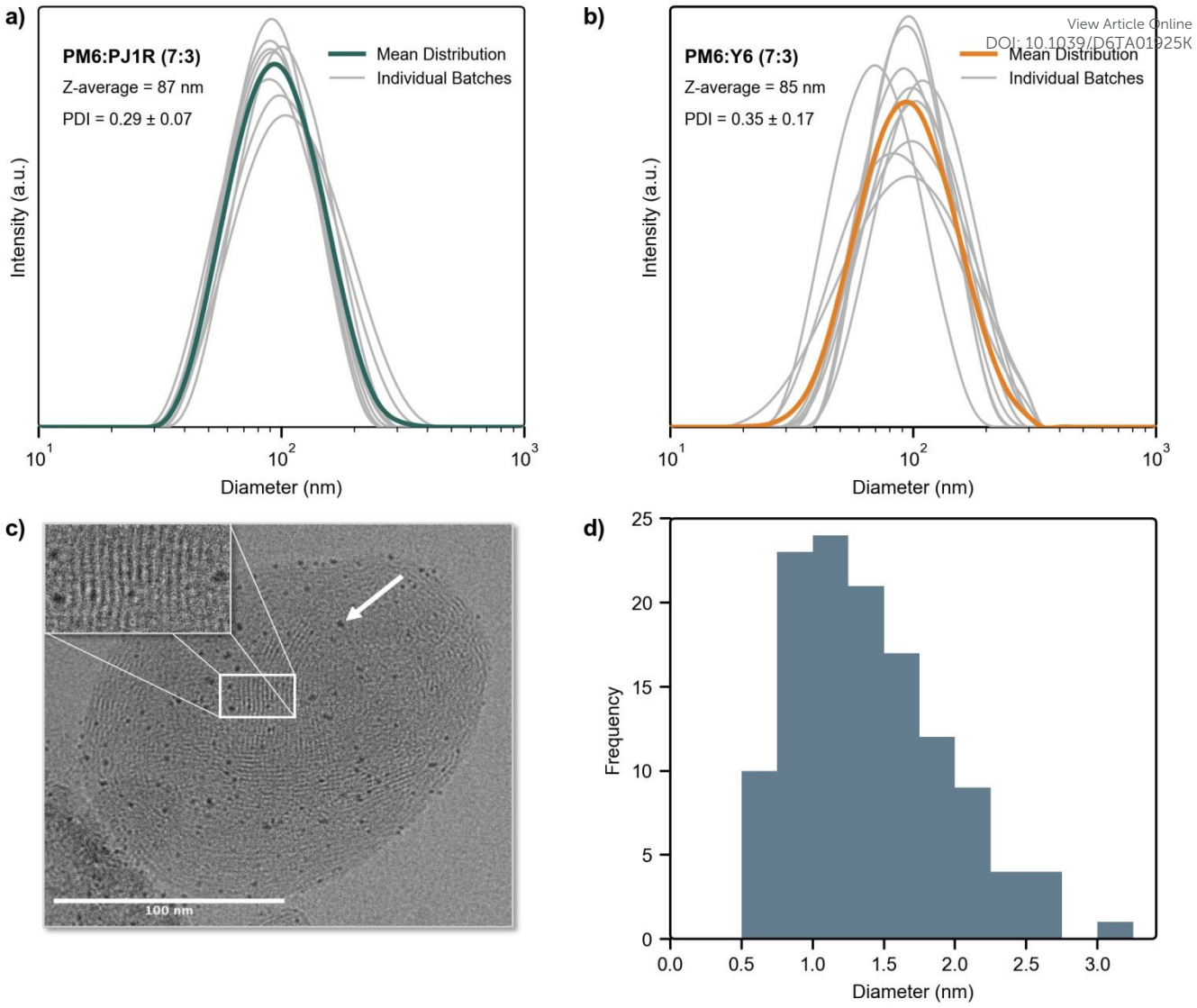

Figure 2. Size distributions of organic nanoparticle samples prepared over 10 different batches along with the mean distribution of all samples, made using the mini-emulsion method, for a) PM6:PJ1-R (7:3) and b) PM6:Y6 (7:3). c) Cryo-TEM image of PM6:PJ1-R (7:3) nanoparticles stabilized by TEBS surfactant with Pt deposited on the surface, indicated by the arrow. The inset shows a region of lamellar stacking, which was identified as PM6. d) Size distribution of Pt nanoparticles on the surface of the PM6:PJ1-R (7:3) nanoparticle, calculated assuming spherical Pt clusters following the method in experimental section (Supplementary Information).

associated with its regiorandom analogue PJ1.[38] PJ1-R (Figure 1a) has a structure similar to PY-IT (Supplementary Information Figure S1), but contains slightly longer branched alkyl chains, improving solubility. PJ1-R was paired with the donor polymer PM6, due to the good reported BHJ device efficiency of over 15%, and the ability to compare the performance to the previously reported PM6:Y6 nanoparticles (Figure 1a).[31] The monomeric unit of PJ1-R is analogous to the high-performing SMA Y6. The structure of Y6 can be described as A'-DAD-A', being made up of alternating electron-rich and electron-deficient regions (D and A, respectively).[39] Subtle structural differences between the Y6 small molecule and the PJ1-R polymeric acceptor can influence their respective packing motifs and energetic properties in nanoparticles. Compared to Y6, PJ1-R incorporates longer alkyl side chains, lacks electron-withdrawing fluorine atoms on the terminal DFIC units, and contains an additional thiophene co-monomer within the backbone (Figure 1a). These modifications collectively hinder backbone planarity and introduce steric hindrance, leading to a suppression of long-range π–π stacking and a higher degree of conformational disorder. The omission of fluorine atoms weakens non-covalent interactions that typically promote planarization and tight molecular packing in Y6 and simultaneously raises the LUMO energy level due to reduced electron-withdrawing strength. Moreover, the thiophene comonomer acts as a spacer which introduces torsional freedom, disrupting the extended conjugation pathway and impeding crystallinity.

The organic nanoparticles were fabricated via a mini-emulsion method, in which the nascent particles are stabilised by the surfactant 2-(3-thienyl)ethyloxybutylsulfonate (TEBS).[20] Our procedure (outlined in Figure 1b and detailed in the experimental section) was adapted from previous reports.[20–22] We initially started with a 7:3 ratio of PM6:Y6, as noted in the previous study, and replaced Y6 with PJ1-R. Although working blends could be formed, we observed poor

View Article Online
DOI: 10.1039/D6TA01925K

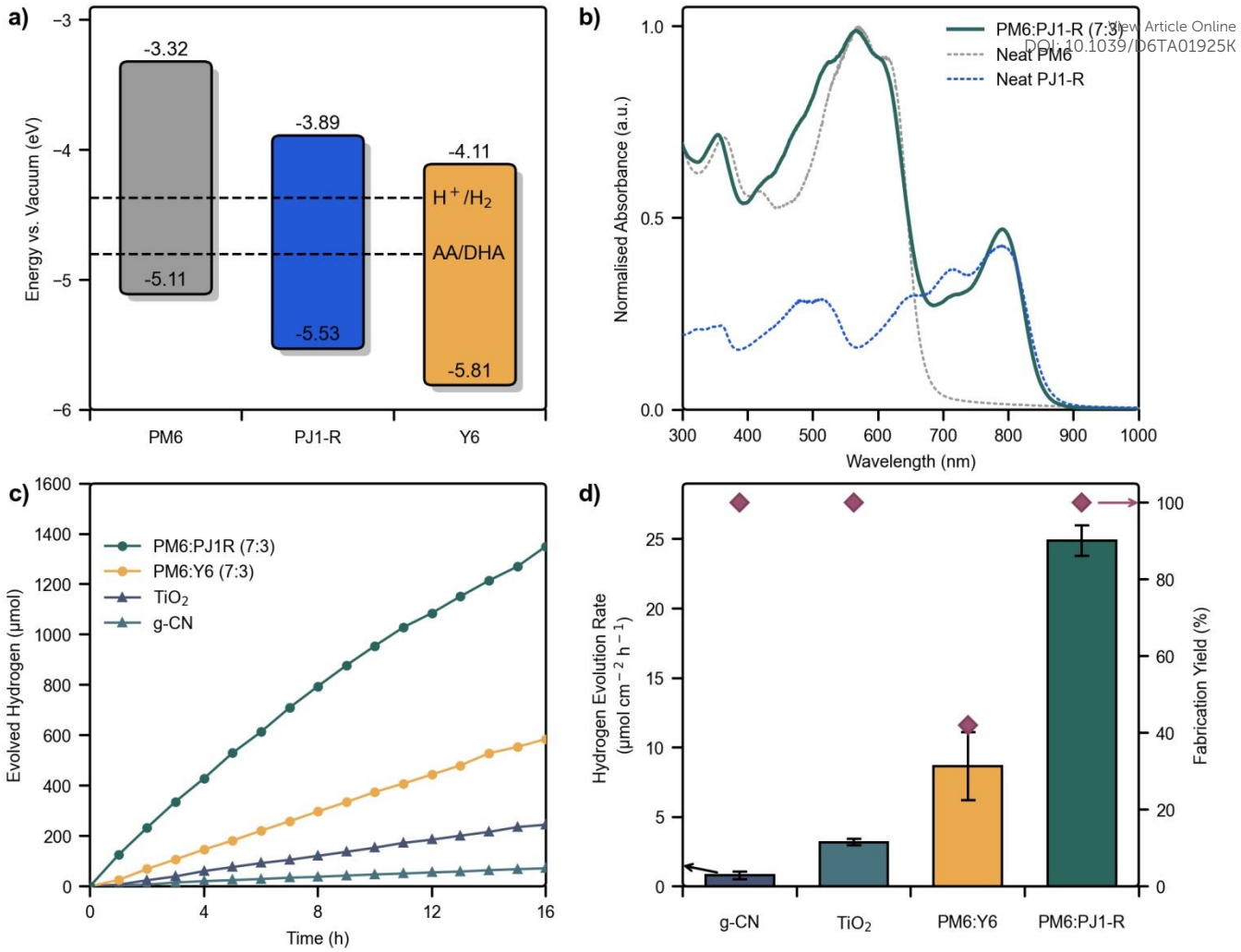

Figure 3. a) Energy levels of highest occupied molecular orbital (HOMO) and lowest unoccupied molecular orbital (LUMO) of PM6, PJ1-R, (measured by UPS/IPES, Supplementary Figure S4) and literature value of Y6[40], along with the reduction potentials of hydrogen and ascorbic acid (AA) calculated at pH 2. b) Normalised UV-VIS spectra for neat PM6, neat PJ1-R and PM6:PJ1-R (7:3) blend. Spectra normalized according to the relative blend ratios of the optimal blend. c) Hydrogen evolution rate over time for optimal samples of PM6:PJ1-R, PM6:Y6, TiO2, and g-CN. d) Comparison of optimal HER rates and fabrication yield of different photocatalysts. Fabrication yield is defined as the % of batches which do not see aggregation issues and are photoactive to a minimum of 80% of the optimal rate. g-CN and TiO2 had Pt loading of 1 and 1.5%, respectively, and used TEOA as sacrificial reagent in place of AA.

reproducibility in the performance of PM6:Y6 and therefore investigated multiple parameters in an effort to afford reproducible nanoparticle formation. Out of the various variables, several were found to be critical. In particular, insufficient stirring prior to sonication led to poorly emulsified systems and ultimately poorly performing batches. Additionally, the depth of the sonicator tip into the solution proved essential, with immersion too deep into the emulsion causing foaming, increasing the likelihood of aggregation.

After the optimisation process it was clear that nanoparticles prepared from PM6:PJ1-R blends exhibited more uniform sizes and distributions (mean PDI = 0.29 ± 0.07) compared to those from PM6:Y6 systems (mean PDI = 0.35 ± 0.17), as shown in Figure 2a and 2b. The significant difference in distribution was attributed to the higher crystallinity of SMAs like Y6, which can induce phase segregation and disrupt morphological uniformity.

In contrast, the reduced crystallinity and more amorphous character of the PSMA blend is expected to promote finer donor-acceptor intermixing within the bulk heterojunction, leading to a more uniform surface morphology. This increased uniformity may minimise the number of exposed crystalline acceptor domains that serve as nucleation sites for flocculation or preferential Pt deposition. Qualitative observations also support this conclusion: PM6:Y6 nanoparticles often exhibited visible aggregation immediately after fabrication, whereas PM6:PJ1-R nanoparticles remained well-dispersed, even after storage for 12 months.

Cryogenic transmission electron microscopy (cryo-TEM) was conducted to help assess the morphology of the samples. Both PM6:Y6 and PM6:PJ1-R exhibit spherical nanoparticle formation in the presence of TEBS (Supplementary Figures S2 and S3 show more examples). Figure 2c is representative, showing an intermixed, BHJ morphology of PM6:PJ1-R nanoparticles decorated with Pt clusters.

View Article Online
DOI: 10.1039/D6TA01925K

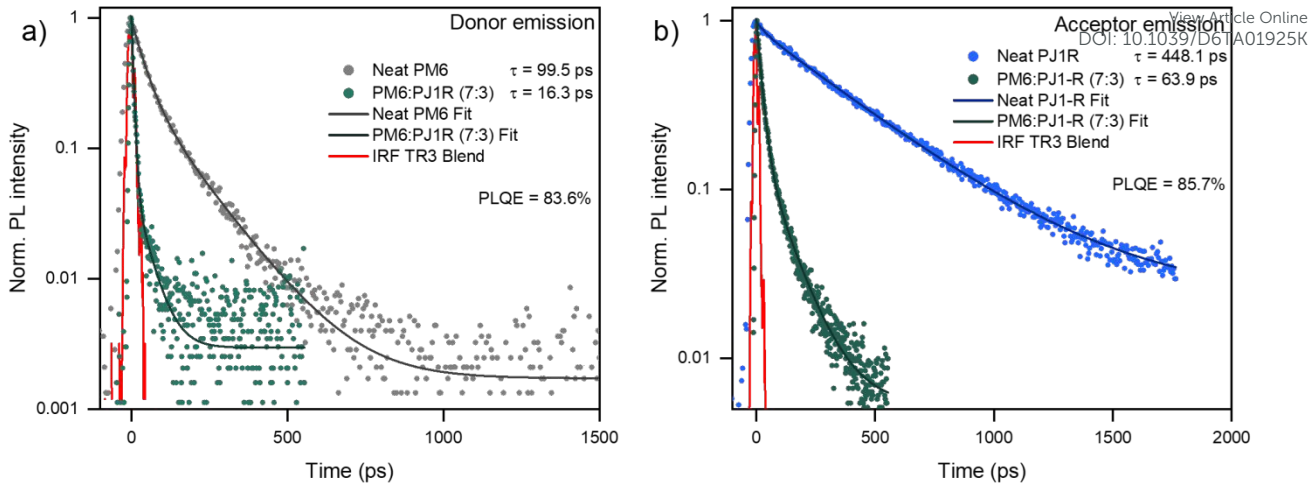

Figure 4. Normalized TrPL decay kinetics from (a) donor emission (integrated over 680 nm - 720 nm) and (b) acceptor emission (integrated over 840 nm - 890 nm) for the neat and blend nanoparticles with an excitation wavelength of 500 nm. Overlaid as solid lines are bi-exponential fits to the decay curves, where the lifetime (τ) values shown are intensity averages.

The Pt was observed to be distributed on the surface as small clusters with a narrow size distribution (1.67 ± 0.52 nm diameter, Figure 2d). For PM6:PJ1-R nanoparticles, Pt deposition was observed to preferentially occur on the acceptor rich regions of the surface, similar to previous reports on PM6:Y6.[21] This was confirmed by comparing the packing distances of the blend with that of neat PJ1-R and neat PM6 nanoparticles, which were found to have significantly different packing distances of 2.10 ± 0.17 nm, and 2.41 ± 0.07 nm, respectively (Supplementary Figure S5 and S6). PM6 nanoparticles formed well-ordered lamellar stacks while PJ1-R lacked long range order. Instead of aligned lamellae or fibrillar domains, the packing appeared disordered and lacked a preferred orientation. This is supported by fast Fourier transform (FFT) analysis, which show concentric ring patterns - indicative of isotropic short-range order rather than crystalline domains.

Determination of the extinction coefficient of PJ1-R enabled accurate assessment of nanoparticle suspension concentrations via absorption spectroscopy. Immediately after fabrication of pristine PJ1-R nanoparticles, with no visible aggregation of the sample, a dilution series was made. Measuring the absorbance at 795 nm gave a calculated extinction coefficient of 45.2 mL mg^{-1} cm^{-1} (Supplementary S7). It was found that the discrepancy between assumed mass and measured mass was approximately 0.15 mg, for samples prepared with 2.5 mg nanoparticles. This difference likely stemmed from material loss between transfers, and we note it can cause significant variations in the calculation of the rate of catalysis (often expressed as mmol g^{-1} h^{-1}). For this reason, our rates are quoted as amount of hydrogen produced per area of surface illumination in units of µmol cm^{-2} h^{-1}.

Hydrogen evolution rates of both PM6:PJ1-R and PM6:Y6 nanoparticles were measured using a calibrated gas chromatography setup, detailed in Supplementary Figure S8, with the data shown in Figure 3 and S9. The energy levels of the materials (Figure 3a) show that PJ1-R has a narrower band gap, and shallower lying frontier molecular orbitals, relative to Y6. Structural differences between PJ1-R and Y6 directly influence the HOMO-LUMO of the PSMA. The removal of the end-capping fluorine atoms and the addition of the electron rich thiophene co-monomer results in a shallower LUMO and therefore provide a higher overpotential relative to Y6. This could contribute thermodynamically to the higher observed rate of reaction. Optical analyses were also undertaken, with the absorption spectra in Figure 3b, and photoluminescence spectra shown in Supplementary S10-S13. The absorption spectrum of PJ1-R is complementary to that of PM6, showing strong absorption between 650-850 nm and lower absorption around 550 nm, the latter near the absorption maximum of PM6. The absorbance spectra of the optimised PM6:Y6 blend and neat Y6 nanoparticles are shown in Supplementary Figure S14. Neat Y6 NPs exhibit a slightly smaller optical band gap, with an onset at 910 nm and λ_{max} at 829 nm, compared to 862 nm and 795 nm for neat PJ1-R NPs. Interestingly, upon blending with PM6 there is pronounced blue-shift for Y6 region, shifting to an onset of 900 nm and λ_{max} at 801 nm, which is largely absent for PJ1-R blends (λ_{onset} at 852 nm and λ_{max} at 795 nm). We attribute these differences to the high crystallinity of the SMA, which is disrupted upon blending.

For both PM6:Y6 and PM6:PJ1-R systems, we also investigated the influence of donor-acceptor ratio on hydrogen production. In agreement with the previous study, PM6:Y6 optimised at a 7:3 ratio, as did the all-polymer system (Supplementary Figure S15). The optimum Pt loading for PM6:PJ1-R was found to be 10 wt% (Supplementary S16), the same as for PM6:Y6[21]. Under sacrificial conditions with ascorbic acid (AA), the optimal rate of reaction for PM6:PJ1-R was 24.89 ± 1.08 µmol cm^{-2} h^{-1}, or 45.9 ± 1.8 mmol g^{-1} h^{-1}, which is nearly 2.5× the reported optimum of PM6:Y6 at 9.9 ± 1.0 µmol cm^{-2} h^{-1}.[21] Our measured rate agrees well with the reported value, although it is worth highlighting the low fabrication yield. The small standard deviation for the PM6:PJ1-R nanoparticles further highlights their high degree of reproducibility and consistent performance. Figure 3c shows the cumulative amount of hydrogen produced over 16 hours of illumination under AM1.5G at 1 sun intensity, comparing g-CN, TiO_2, PM6:Y6, and PM6:PJ1-R. These systems were illuminated under 1 sun over a broad spectrum (240 – 1200 nm) to simulate deployment using natural sunlight and allows for comparison to alternative photocatalytic systems. Figure 3d shows how the fabrication yield (defined as the

View Article Online DOI: 10.1039/D6TA01925K

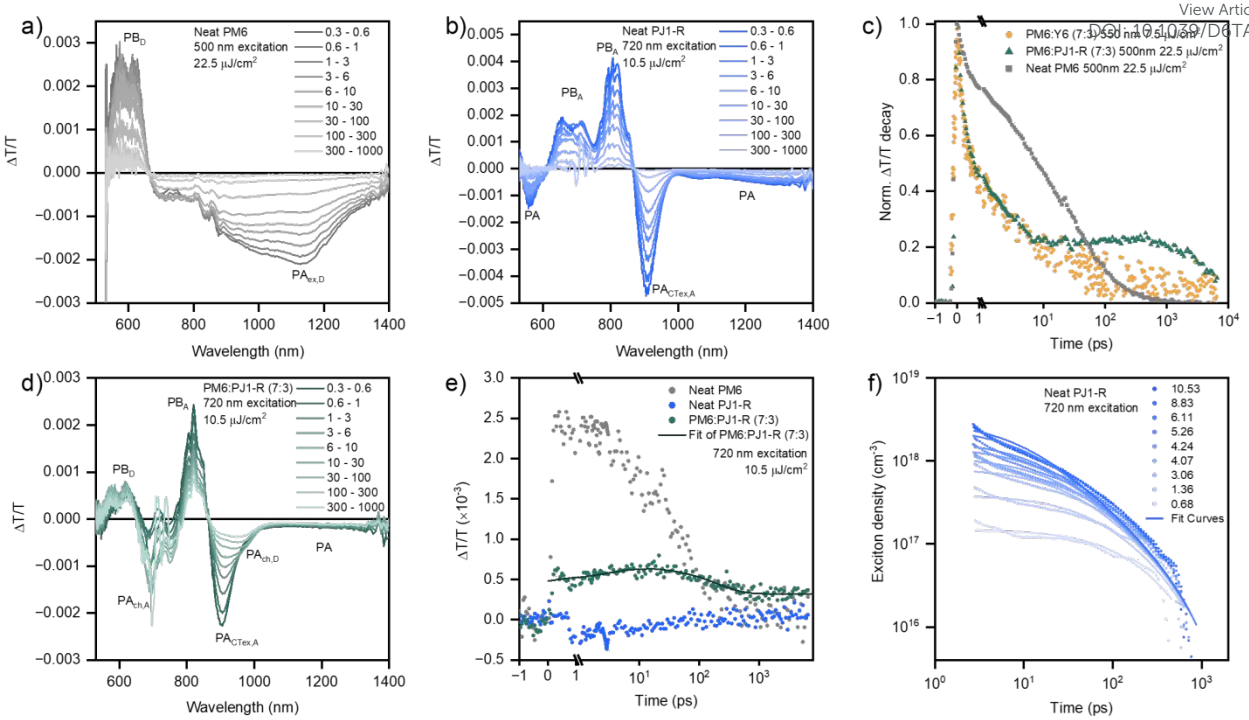

Figure 5. Transient absorption spectra for nanoparticles excited for different pump-probe time delays (in picoseconds): a) neat PM6 nanoparticles excited at 500 nm; b) neat PJ1-R nanoparticles excited at 720 nm; c). Normalised kinetics of the PM6 photoinduced absorption (PA) signal (integrated over 1140 nm to 1160 nm) for PM6:Y6 (7:3), PM6:PJ1-R (7:3), and neat PM6 nanoparticles. Data of PM6:Y6 are obtained from the publication by Kosco et al. (ref.[21]) d) TA of PM6:PJ1-R (7:3) nanoparticles excited at 720 nm e) Kinetics of the PM6 photobleach (PB) signal (integrated over 600 nm to 620 nm) for neat PM6, neat PJ1-R, and PM6:PJ1-R (7:3) nanoparticles, showing the diffusion-limited hole transfer timescale. f) Fluence-dependent kinetics (μJ cm^{-2}) of the neat PJ1-R PA signal (integrated over 880 nm to 950 nm), excited at 720 nm. Overlaid as solid lines are best fit results from a global fit to the singlet exciton-singlet exciton annihilation model.

percentage of nanoparticle batches that show no aggregation and perform above 80% of the optimum hydrogen evolution rate)[22] of the all-polymer nanoparticles is 100% (over 16 samples), the same as that of commercial TiO_2 and g-C_3N_4. In contrast the optimised PM6:Y6 samples prepared for this study still showed significant variation in performance, size distributions, and stability towards aggregation. This is reflected in a poor fabrication yield of 42% (over 14 samples).

Spectroscopic characterisation of the nanoparticles was performed to further investigate the reasons for the high rate of hydrogen production. Time-resolved photoluminescence (TRPL) spectroscopy was employed to determine the exciton lifetime (τ_{ex}) of the nanoparticle suspensions by fitting the decay kinetics using bi-exponential functions, where τ_{ex} was taken as the intensity-average. The PL spectra as a function of decay time are shown in Supplementary Figure S17. As shown in Figure 4a, neat PM6 nanoparticles show a lifetime of 99.5 ps, while the donor emission from PM6:PJ1-R blend nanoparticles exhibit a much shorter lifetime of 16.3 ps, resulting in a photoluminescence quenching efficiency (PLQE) of 83.6%, calculated using the equation:

$$\mathbf{PLQE} = \mathbf{1} - \frac{\boldsymbol{\tau}_{\mathbf{blend}}}{\boldsymbol{\tau}_{\mathbf{neat}}}$$

This value is nearly double the reported 44.9% for PM6:Y6 nanoparticles[22] due to a more efficient energy transfer from PM6 to PJ1-R, likely arising from better inter-mixing between PM6 and the PSMA, as well as stronger spectral overlap between the emission of PM6 and absorption of PJ1-R. This high quenching efficiency quantitatively supports our earlier hypothesis that the polymeric acceptor prevents the formation of large, phase-separated crystalline domains, which were observed to hinder performance in the PM6:Y6 system. For acceptor emission, the exciton lifetime of neat PJ1-R nanoparticles was reduced from 448.1 ps in neat nanoparticles to 63.9 ps in PM6:PJ1-R blend nanoparticles (Figure 4b). The higher PLQE of 85.7% for PM6:PJ1-R nanoparticles indicates superior exciton-to-charge conversion compared with PM6:Y6 nanoparticles (72.6%).[41] We note that neat PJ1-R nanoparticles also retain a relatively high PL quantum yield (1.76%) compared to PM6 nanoparticles (0.24%), despite their narrow bandgap, near-infrared emission (Supplementary Figure S18).

To probe the charge carrier dynamics of the donor-acceptor system, transient absorption (TA) spectroscopy was employed. Under 500 nm excitation, the neat PM6 nanoparticles demonstrated a photobleach (PB) signal at 550 nm - 650 nm and a broad photoinduced absorption (PA) signal from 850 nm – 1400 nm, with the maximum at 1150 nm (Figure 5a). These signals are characteristic to PM6, and the signal has been previously attributed to PA by singlet excitons (PA_{ex}).[21,42] The neat PJ1-R nanoparticles were excited with a wavelength of 720 nm, and demonstrated 2 distinct PB bands in the range of 650 nm - 850 nm, with 3 PA bands at 550 nm - 600 nm, 870 nm - 980 nm, and 1000 nm - 1400 nm (Figure 5b). The spectral features of PJ1-R nanoparticles were very similar to those of Y6

nanoparticles[21,22] and films[43–45], where the dominant PA band centred at 910 nm has been attributed to a hybrid charge transfer (CT)-exciton species (PA_{CTex}).[43] In the PM6:PJ1-R blend, when excited at 500 nm, PB signals from both the donor (PB_D) and acceptor (PB_A) were present, and there were 3 dominant PA bands between 650 nm – 785 nm, 870 nm – 1000 nm, and 1040 nm – 1300 nm (Supplementary Figure S19a). The negative ΔT/T bands at 650 nm – 785 nm have been attributed to PA from charges in the acceptor[43,46] ($PA_{ch,A}$) for the peak centered at 750 nm, as confirmed by spectroelectrochemistry experiments[47] on Y6, and electroabsorption from PM6 (EA_D) for the peak centered at 685 nm[46]. The PA band at 870 nm – 1000 nm is a convolution of the PA_{CTex} of PJ1-R superimposed on the overlapping charge absorption by both PM6[46,47] ($PA_{ch,D}$) and PJ1-R. Finally, the PA band centred around 1130 nm corresponds to PA_{ex} from PM6, similar to that of the neat PM6 nanoparticles. The identities of each of the long-lived species, arising from charges, EA, and/or triplet states, were further confirmed using nanosecond-microsecond TA measurements (Figure S19b).

The PA_{ex} signal from neat PM6 nanoparticles decayed with an amplitude-averaged lifetime of 32.8 ps using a bi-exponential decay fitting, which was reduced to 3.9 ps when blended with PJ1-R (Figure 5c). This rapid reduction of the PA_{ex} lifetime indicates efficient energy transfer from PM6 to PJ1-R which occurs at this timescale.[41] Compared with PM6:Y6 nanoparticles, the PA_{ex} had similar lifetime, demonstrating that energy transfer occurred at similar timescales for both systems. The long-lived tail from PM6:PJ1-R nanoparticles arose from additional broad PA_{ch} species centred at ~1400 nm forming at longer timescales. To investigate hole transfer from PJ1-R to PM6, the acceptor was selectively excited at 720 nm (Figure 5d). The TA spectra were dominated predominantly by features of PJ1-R at early timescales, although the PB_D from PM6 was also present at earliest timescales, indicating ultrafast hole transfer from PJ1-R to PM6 occurred at sub-120 fs timescales. As charge separation occurs orders of magnitude faster than the catalytic turnover, this suggests that the rate-limiting step for hydrogen evolution in this system is surface catalysis, not charge generation. The $PA_{ch,D}$ signal at ~950 nm became more pronounced with longer pump-probe delay times. As expected, there was no $PA_{ex,D}$ signature present when exciting at 720 nm, unlike when directly exciting PM6 (Supplementary Figure S19). Hole transfer kinetics were obtained by probing the PB_D peak at 610 nm (Figure 5e). Since PJ1-R featured an isosbestic point around 0 at this wavelength, the signal came predominantly from the ground state PB of PM6. As there was already a signal of ~0.5×10^{-3} at the earliest timescales, some fraction of holes transferred from PJ1-R to PM6 at sub-120 fs timescales. Using an exponential growth-decay function to fit, the signal continued to rise up to 17.4 ps, accounting for the time additional PJ1-R excitons took to diffuse to the donor:acceptor interface prior to hole transfer.[48–50]

To further evaluate the exciton diffusion within PJ1-R nanoparticles, fluence-dependent TA kinetics of neat PJ1-R nanoparticles were measured under 720 nm excitation (Figure 5f). The signal intensities were converted into exciton densities, which were then fit with the singlet-singlet annihilation (SSA) model (detailed in Supplementary Information Experimental and Figure S20).[51,52] From the fits, a bimolecular SSA rate constant (α) of 6.9×10^{-8} cm^3/s was obtained. Accordingly, an exciton diffusion coefficient (D_{ex}) of 2.6×10^{-2} cm^2/s was calculated using a singlet exciton annihilation radius (R_A) of 1 nm, and, taking an τ_{ex} of 448.1ps, an exciton diffusion length of 35 ± 4.2 nm was calculated. Given that the hole transfer timescale (τ_{HT}) occurred at 17.4 ps, the PJ1-R domain size (L'_D) within the blend nanoparticles can be estimated by:

$$\mathbf{L'_D} = \sqrt{\mathbf{D} \cdot \boldsymbol{\tau}_{\mathbf{HT}}}$$

giving an L'_D of 6.9 ± 0.8 nm. This domain size is significantly smaller than the typical exciton diffusion length, confirming that the 'intermixed' morphology observed in Cryo-TEM (Figure 2c) creates a donor-acceptor network that is highly favourable for exciton dissociation. Therefore, we conclude that the efficient energy transfer process from PM6 to PJ1-R, coupled with the fast hole transfer from PJ1-R to PM6 and the small PJ1-R domain sizes, account for the high exciton-to-charge conversion efficiency for these nanoparticles, and subsequently the fast rate of hydrogen evolution.

Conclusion

This study demonstrates the successful fabrication of all-polymer BHJ nanoparticles for application in sacrificial photocatalytic hydrogen evolution. Comparative evaluation between nanoparticles based on polymer PM6 and the benchmark acceptor molecule, Y6, with its polymeric analogue, PJ1-R, revealed a substantial enhancement in catalytic activity for the all-polymer system across all investigated blend ratios. Notably, the optimal catalytic performance was achieved with a PM6:PJ1-R ratio of 7:3, yielding a hydrogen evolution rate of 24.89 μmol cm^{-2} h^{-1}. This represents an approximate improvement of 2.5-fold compared to the PM6:Y6 (7:3) blend (9.9 μmol cm^{-2} h^{-1}). Importantly, the preparation of the all-polymer nanoparticles was shown to be highly controlled and reproducible. Furthermore, nanoparticle sizes were consistently maintained within a narrow z-average diameter range of 80–120 nm. Hydrogen evolution rates for the all-polymer nanoparticles exhibited excellent reproducibility, with minimal deviations in the rate of photocatalysis (± 8% H_2 evolution rate) observed around the optimal blend ratio. TEM analysis of the nanoparticles provided evidence that an intermixed morphology between PJ1-R and PM6 was present in the all-polymer blend, with small regions of local order corresponding to lamellar stacking of PM6.

Spectroscopic analysis revealed that the optimum blend for the all-polymer nanoparticles showed high photoluminescence quenching efficiencies of 84% for donor and 86% for acceptor materials, which is significantly greater than that of PM6:Y6 analogues (45% for donor and 73% for acceptor). Transient absorption spectroscopy revealed efficient energy transfer occurred from PM6 to PJ1-R in sub-picosecond timescales, and that prompt hole transferred from PJ1-R to PM6 occurred at sub-120 fs timescales, whereas excitons generated farther from the interface underwent diffusion-mediated hole transfer on a 17 ps timescale. Exciton diffusion measurements demonstrated the diffusion length of PJ1-R was 35 nm, yielding a domain size of 6.9 nm for PJ1-R within the blend nanoparticles. This yielded an efficient exciton-to-charge conversion efficiency, which gave rise to the fast rate of hydrogen evolution. This work embodies the continued development of highly efficient organic photocatalytic design and fabrication principles, showing a large improvement in catalytic efficiency.

Author contributions

Charles Jeffreys: Methodology, Data Curation, Formal Analysis, Project Administration, Writing – Original Draft, Writing – Review & Editing, Visualisation, Investigation, Conceptualisation. Yakun He: Formal analysis, Methodology, Writing - review & editing, Investigation, Data curation. Nisreen Alshehri: Investigation. Lingyun Zhao: Methodology, Investigation. Adam V. Marsh: Writing – Review & Editing. George T. Harrison: Investigation. Oleksandr Matiash: Methodology. Aren Yazmaciyan: Methodology. Christopher E. Petoukhoff: Writing - original draft, Writing - Review & Editing, Formal Analysis, Validation, Supervision, Project administration. Shadi Fatayer: Supervision, Resources, Validation, Writing - Review & Editing, Funding Acquisition. Frédéric Laquai: Supervision, Resources, Funding Acquisition, Validation, Writing - Review & Editing. Martin Heeney: Supervision, Resources, Funding Acquisition, Validation, Writing - Review & Editing, Conceptualisation, Methodology.

Conflicts of interest

There are no conflicts to declare.

Acknowledgements

This publication is based on work supported by the KAUST Office of Sponsored Research (OSR) under award numbers ORFS-CRG11-2022-5045 and ORFS-CRG12-2024-6443. C.E.P. acknowledges support from KAUST Global Fellowship Program (KGFP) under Award No. ORA-2022-5002. Y.K.H. acknowledges the support from KGFP under Award No. ORA-2023-6014.

References

(1) Halder, P.; Babaie, M.; Salek, F.; Haque, N.; Savage, R.; Stevanovic, S.; Bodisco, T. A.; Zare, A. Advancements in Hydrogen Production, Storage, Distribution and Refuelling for a Sustainable Transport Sector: Hydrogen Fuel Cell Vehicles. *Int. J. Hydrog. Energy* **2024**, *52*, 973–1004. https://doi.org/10.1016/j.ijhydene.2023.07.204.

(2) Hosseini, S. E. Hydrogen Fuel, a Game Changer for the World's Energy Scenario. *Int. J. Green Energy* **2024**, *21* (6), 1366–1382. https://doi.org/10.1080/15435075.2023.2244050.

(3) Jiao, K.; Xuan, J.; Du, Q.; Bao, Z.; Xie, B.; Wang, B.; Zhao, Y.; Fan, L.; Wang, H.; Hou, Z.; Huo, S.; Brandon, N. P.; Yin, Y.; Guiver, M. D. Designing the next Generation of Proton-Exchange Membrane Fuel Cells. *Nature* **2021**, *595* (7867), 361–369. https://doi.org/10.1038/s41586-021-03482-7.

(4) Agyekum, E. B.; Nutakor, C.; Agwa, A. M.; Kamel, S. A Critical Review of Renewable Hydrogen Production Methods: Factors Affecting Their Scale-Up and Its Role in Future Energy Generation. *Membranes* **2022**, *12* (2), 173. https://doi.org/10.3390/membranes12020173.

(5) Gupta, A.; Likozar, B.; Jana, R.; Chanu, W. C.; Singh, M. K. A Review of Hydrogen Production Processes by Photocatalytic Water Splitting – From Atomistic Catalysis Design to Optimal Reactor Engineering. *Int. J. Hydrog. Energy* **2022**, *47* (78), 33282–33307. https://doi.org/10.1016/j.ijhydene.2022.07.210.

(6) B., A.; A., J.; Rao, A. S.; Nagarkar, S. S.; Dutta, A.; Duttagupta, S. P.; Prabhu, S. S.; Pinto, R. Challenges in Photocatalytic Hydrogen Evolution: Importance of Photocatalysts and Photocatalytic Reactors. *Int. J. Hydrog. Energy* **2024**, *81*, 1442–1466. https://doi.org/10.1016/j.ijhydene.2024.07.262.

(7) Fujishima Akira; Honda, K. Electrochemical Photolysis of Water at a Semiconductor Electrode. *Nature* **1972**, *238* (5358), 37–38. https://doi.org/10.1038/238037a0.

(8) Takata, T.; Jiang, J.; Sakata, Y.; Nakabayashi, M.; Shibata, N.; Nandal, V.; Seki, K.; Hisatomi, T.; Domen, K. Photocatalytic Water Splitting with a Quantum Efficiency of Almost Unity. *Nature* **2020**, *581* (7809), 411–414. https://doi.org/10.1038/s41586-020-2278-9.

(9) Bai, Y.; Hippalgaonkar, K.; Sprick, R. S. Organic Materials as Photocatalysts for Water Splitting. *J. Mater. Chem. A* **2021**, *9* (30), 16222–16232. https://doi.org/10.1039/D1TA03710B.

(10) Sprick, R. S.; Bonillo, B.; Clowes, R.; Guiglion, P.; Brownbill, N. J.; Slater, B. J.; Blanc, F.; Zwijnenburg, M. A.; Adams, D. J.; Cooper, A. I. Visible-Light-Driven Hydrogen Evolution Using Planarized Conjugated Polymer Photocatalysts. *Angew. Chem. Int. Ed.* **2016**, *55* (5), 1792–1796. https://doi.org/10.1002/anie.201510542.

(11) Li, Q.; Jin, W.; Chu, M.; Zhang, W.; Gu, J.; Shahid, B.; Chen, A.; Yu, Y.; Qiao, S.; Zhao, Y. S. Tailoring the Structures and Photonic Properties of Low-Dimensional Organic Materials by Crystal Engineering. *Nanoscale* **2018**, *10* (10), 4680–4685. https://doi.org/10.1039/C7NR08228B.

(12) Liu, Z.; Xie, C.; Heumueller, T.; McCulloch, I.; Brabec, C. J.; Huang, F.; Cao, Y.; Li, N. A Review on Organic Nanoparticle-Based Optoelectronic Devices: From Synthesis to Applications. *Energy Environ. Sci.* **2025**, 18, 155-193. https://doi.org/10.1039/D4EE03575E.

(13) Guo, J.; Zhen, Y.; Dong, H.; Hu, W. Recent Progress on Organic Exciplex Materials with Different Donor–Acceptor Contacting Modes for Luminescent Applications. *J. Mater. Chem. C* **2021**, *9* (47), 16843–16858. https://doi.org/10.1039/D1TC04330G.

(14) Yu, G.; Gao, J.; Hummelen, J. C.; Wudl, F.; Heeger, A. J. Polymer Photovoltaic Cells: Enhanced Efficiencies via a Network of Internal Donor-Acceptor Heterojunctions. *Science* **1995**, *270* (5243), 1789–1791. https://doi.org/10.1126/science.270.5243.1789.

(15) Cao, W.; Xue, J. Recent Progress in Organic Photovoltaics: Device Architecture and Optical Design. *Energy Environ. Sci.* **2014**, *7* (7), 2123. https://doi.org/10.1039/c4ee00260a.

(16) Solak, E. K.; Irmak, E. Advances in Organic Photovoltaic Cells: A Comprehensive Review of Materials, Technologies, and Performance. *RSC Adv.* **2023**, *13* (18), 12244–12269. https://doi.org/10.1039/D3RA01454A.

(17) Li, Y.; Huang, W.; Zhao, D.; Wang, L.; Jiao, Z.; Huang, Q.; Wang, P.; Sun, M.; Yuan, G. Recent Progress in Organic Solar Cells: A Review on Materials from Acceptor to Donor. *Molecules* **2022**, *27* (6), 1800. https://doi.org/10.3390/molecules27061800.

(18) Chen, H.; Huang, Y.; Zhang, R.; Mou, H.; Ding, J.; Zhou, J.; Wang, Z.; Li, H.; Chen, W.; Zhu, J.; Cheng, Q.; Gu, H.; Wu, X.; Zhang, T.; Wang, Y.; Zhu, H.; Xie, Z.; Gao, F.; Li, Y.; Li, Y. Organic Solar Cells with 20.82% Efficiency and High Tolerance of Active Layer Thickness through Crystallization Sequence Manipulation. *Nat. Mater.* **2025**, *24* (3), 444–453. https://doi.org/10.1038/s41563-024-02062-0.

(19) Li, C.; Song, J.; Lai, H.; Zhang, H.; Zhou, R.; Xu, J.; Huang, H.; Liu, L.; Gao, J.; Li, Y.; Jee, M. H.; Zheng, Z.; Liu, S.; Yan, J.; Chen, X.-K.; Tang, Z.; Zhang, C.; Woo, H. Y.; He, F.; Gao, F.; Yan, H.; Sun, Y. Non-Fullerene Acceptors with High Crystallinity and Photoluminescence Quantum Yield Enable >20% Efficiency Organic Solar Cells. *Nat. Mater.* **2025**, *24* (3), 433–443. https://doi.org/10.1038/s41563-024-02087-5.

(20) Kosco, J.; Bidwell, M.; Cha, H.; Martin, T.; Howells, C. T.; Sachs, M.; Anjum, D. H.; Gonzalez Lopez, S.; Zou, L.; Wadsworth, A.; Zhang, W.; Zhang, L.; Tellam, J.; Sougrat, R.; Laquai, F.; DeLongchamp, D. M.; Durrant, J. R.; McCulloch, I. Enhanced Photocatalytic Hydrogen Evolution from Organic Semiconductor Heterojunction Nanoparticles. *Nat. Mater.* **2020**, *19* (5), 559–565. https://doi.org/10.1038/s41563-019-0591-1.

(21) Kosco, J.; Gonzalez-Carrero, S.; Howells, C. T.; Fei, T.; Dong, Y.; Sougrat, R.; Harrison, G. T.; Firdaus, Y.; Sheelamanthula, R.; Purushothaman, B.; Moruzzi, F.; Xu, W.; Zhao, L.; Basu, A.; De Wolf, S.; Anthopoulos, T. D.; Durrant, J. R.; McCulloch, I. Generation of Long-Lived Charges in Organic Semiconductor Heterojunction Nanoparticles for Efficient Photocatalytic Hydrogen Evolution. *Nat. Energy* **2022**, *7* (4), 340–351. https://doi.org/10.1038/s41560-022-00990-2.

(22) Ferree, M.; Kosco, J.; Alshehri, N.; Zhao, L.; De Castro, C. S. P.; Petoukhoff, C. E.; McCulloch, I.; Heeney, M.; Laquai, F. Organic Semiconductor Nanoparticles for Visible-Light-Driven CO_2 Conversion. *Sustain. Energy Fuels* **2024**, *8* (11), 2423–2430. https://doi.org/10.1039/D4SE00196F.

(23) Dolan, A.; De La Perrelle, J. M.; Small, T. D.; Milsom, E. R.; Metha, G. F.; Pan, X.; Andersson, M. R.; Huang, D. M.; Kee, T. W. Surfactant Effects on Hydrogen Evolution by Small-Molecule Nonfullerene Acceptor Nanoparticles. *ACS Appl. Nano Mater.* **2022**, *5* (9), 12154–12164. https://doi.org/10.1021/acsanm.2c02350.

(24) Yang, Y.; Li, D.; Cai, J.; Wang, H.; Guo, C.; Wen, S.; Li, W.; Wang, T.; Liu, D. Enhanced Photocatalytic Hydrogen Evolution from Organic Ternary Heterojunction Nanoparticles Featuring a Compact Alloy-Like Phase. *Adv. Funct. Mater.* **2023**, *33* (10), 2209643. https://doi.org/10.1002/adfm.202209643.

(25) Wen, S.; Yang, Y.; Cai, J.; Guo, C.; Wang, H.; Chen, C.; Liu, Y.; Zhang, X.; Li, D.; Chen, Z.; Li, W.; Wang, T.; Liu, D. Molecular Structure Engineering toward Enhanced Photocatalytic Hydrogen Evolution and Stability of Organic Heterojunction Nanoparticles. *ACS Catal.* **2023**, *13* (19), 12730–12736. https://doi.org/10.1021/acscatal.3c02932.

(26) Missaoui, K.; Wantz, G.; Toupance, T.; Chambon, S.; Kuhn, A. Targeted Design of Organic Janus Particles for Improved Photocatalytic Hydrogen Evolution. *Chem. Sci.* **2025**, *16* (24), 10691–10700. https://doi.org/10.1039/D5SC00802F.

(27) Li, X.-J.; Sun, G.-P.; Gong, Y.-F.; Li, Y.-F. Recent Research Progress of N-Type Conjugated Polymer Acceptors and All-Polymer Solar Cells. *Chin. J. Polym. Sci.* **2023**, *41* (5), 640–651. https://doi.org/10.1007/s10118-023-2944-0.

(28) Lv, J.; Chen, J.; Liu, B.; Guo, X. Recent Advances of Polymer Acceptors for Efficient All-Polymer Solar Cells. *Chem. Commun.* **2025**, *61* (61), 11382–11400. https://doi.org/10.1039/D5CC02880A.

(29) Mistry, J.-R.; McQueen, E.; Nudelman, F.; Sprick, R. S.; Wright, I. A. Non-Conventional Bulk Heterojunction Nanoparticle Photocatalysts for Sacrificial Hydrogen Evolution from Water. *J. Mater. Chem. A* **2024**, *12* (35), 23411–23415. https://doi.org/10.1039/D4TA03584D.

(30) Wang, T.; Chen, M.; Sun, R.; Min, J. Recent Research Progress of All-Polymer Solar Cells Based on PSMA-Type Polymer Acceptors. *Chem* **2023**, *9* (7), 1702–1767. https://doi.org/10.1016/j.chempr.2023.05.031.

(31) Luo, Z.; Liu, T.; Ma, R.; Xiao, Y.; Zhan, L.; Zhang, G.; Sun, H.; Ni, F.; Chai, G.; Wang, J.; Zhong, C.; Zou, Y.; Guo, X.; Lu, X.; Chen, H.; Yan, H.; Yang, C. Precisely Controlling the Position of Bromine on the End Group Enables Well-Regular Polymer Acceptors for All-Polymer Solar Cells with Efficiencies over 15%. *Adv. Mater.* **2020**, *32* (48), 2005942. https://doi.org/10.1002/adma.202005942.

(32) Bai, Q.; Liang, Q.; Liu, Q.; Liu, B.; Guo, X.; Niu, L.; Sun, H. PY-IT , an Excellent Polymer Acceptor†. *Chin. J. Chem.* **2023**, *41* (24), 3714–3728. https://doi.org/10.1002/cjoc.202300404.

(33) Zhang, Z.; Yang, Y.; Yao, J.; Xue, L.; Chen, S.; Li, X.; Morrison, W.; Yang, C.; Li, Y. Constructing a Strongly Absorbing Low-Bandgap Polymer Acceptor for High-Performance All-Polymer Solar Cells. *Angew. Chem. Int. Ed.* **2017**, *56* (43), 13503–13507. https://doi.org/10.1002/anie.201707678.

(34) Mohamed, M. G.; Elsayed, M. H.; Li, C.-J.; Hassan, A. E.; Mekhemer, I. M. A.; Musa, A. F.; Hussien, M. K.; Chen, L.-C.; Chen, K.-H.; Chou, H.-H.; Kuo, S.-W. Reticular Design and Alkyne Bridge Engineering in Donor–π–Acceptor Type Conjugated Microporous Polymers for Boosting Photocatalytic Hydrogen Evolution. *J. Mater. Chem. A* **2024**, *12* (13), 7693–7710. https://doi.org/10.1039/D3TA07309B.

(35) Reyes, Y. I. A.; Ting, L.-Y.; Tu, X.; Chen, H.-Y. T.; Chou, H.-H.; Coluccini, C. Mechanistic Studies of Hydrogen Evolution Reaction on Donor-Acceptor Conjugated Polymer Photocatalysts. *Appl. Sci.* **2020**, *10* (20), 7017. https://doi.org/10.3390/app10207017.

(36) Zhao, J.; Liu, Y.; An, R.; Fu, Y.; Wang, P.; Wu, X.; Tong, H.; Wang, L. Polymerized Small-Molecule Acceptors with Linker Length-Dependent Photocatalytic Activity for High-Performance Solar Hydrogen Evolution. *Adv. Funct. Mater.* **2025**, *35* (22), 2421994. https://doi.org/10.1002/adfm.202421994.

(37) Elsayed, M. H.; Abdellah, M.; Alhakemy, A. Z.; Mekhemer, I. M. A.; Aboubakr, A. E. A.; Chen, B.-H.; Sabbah, A.; Lin, K.-H.; Chiu, W.-S.; Lin, S.-J.; Chu, C.-Y.; Lu, C.-H.; Yang, S.-D.; Mohamed, M. G.; Kuo, S.-W.; Hung, C.-H.; Chen, L.-C.; Chen, K.-H.; Chou, H.-H. Overcoming Small-Bandgap Charge Recombination in Visible and NIR-Light-Driven Hydrogen Evolution by Engineering the Polymer Photocatalyst Structure. *Nat. Commun.* **2024**, *15* (1), 707. https://doi.org/10.1038/s41467-024-45085-6.

(38) Jia, T.; Zhang, J.; Zhong, W.; Liang, Y.; Zhang, K.; Dong, S.; Ying, L.; Liu, F.; Wang, X.; Huang, F.; Cao, Y. 14.4% Efficiency All-Polymer Solar Cell with Broad Absorption and Low Energy Loss Enabled by a Novel Polymer Acceptor. *Nano Energy* **2020**, *72*, 104718. https://doi.org/10.1016/j.nanoen.2020.104718.

(39) Yang, Y. The Original Design Principles of the Y-Series Nonfullerene Acceptors, from Y1 to Y6. *ACS Nano* **2021**, *15* (12), 18679–18682. https://doi.org/10.1021/acsnano.1c10365.

(40) Bertrandie, J.; Han, J.; De Castro, C. S. P.; Yengel, E.; Gorenflot, J.; Anthopoulos, T.; Laquai, F.; Sharma, A.; Baran, D. The Energy Level Conundrum of Organic Semiconductors in Solar Cells. *Adv. Mater.* **2022**, *34* (35), 2202575. https://doi.org/10.1002/adma.202202575.

(41) Karuthedath, S.; Gorenflot, J.; Firdaus, Y.; Chaturvedi, N.; De Castro, C. S. P.; Harrison, G. T.; Khan, J. I.; Markina, A.; Balawi,

A. H.; Peña, T. A. D.; Liu, W.; Liang, R.-Z.; Sharma, A.; Paleti, S. H. K.; Zhang, W.; Lin, Y.; Alarousu, E.; Lopatin, S.; Anjum, D. H.; Beaujuge, P. M.; De Wolf, S.; McCulloch, I.; Anthopoulos, T. D.; Baran, D.; Andrienko, D.; Laquai, F. Intrinsic Efficiency Limits in Low-Bandgap Non-Fullerene Acceptor Organic Solar Cells. *Nat. Mater.* **2021**, *20* (3), 378–384. https://doi.org/10.1038/s41563-020-00835-x.

(42) Karki, A.; Vollbrecht, J.; Gillett, A. J.; Xiao, S. S.; Yang, Y.; Peng, Z.; Schopp, N.; Dixon, A. L.; Yoon, S.; Schrock, M.; Ade, H.; Reddy, G. N. M.; Friend, R. H.; Nguyen, T.-Q. The Role of Bulk and Interfacial Morphology in Charge Generation, Recombination, and Extraction in Non-Fullerene Acceptor Organic Solar Cells. *Energy Environ. Sci.* **2020**, *13* (10), 3679–3692. https://doi.org/10.1039/D0EE01896A.

(43) Giannini, S.; Sowood, D. J. C.; Cerdá, J.; Frederix, S.; Grüne, J.; Londi, G.; Marsh, T.; Ghosh, P.; Duchemin, I.; Greenham, N. C.; Vandewal, K.; D'Avino, G.; Gillett, A. J.; Beljonne, D. On the Role of Charge Transfer Excitations in Non-Fullerene Acceptors for Organic Photovoltaics. *Mater. Today* **2024**, *80*, 308–326. https://doi.org/10.1016/j.mattod.2024.09.009.

(44) Zhu, W.; Spencer, A. P.; Mukherjee, S.; Alzola, J. M.; Sangwan, V. K.; Amsterdam, S. H.; Swick, S. M.; Jones, L. O.; Heiber, M. C.; Herzing, A. A.; Li, G.; Stern, C. L.; DeLongchamp, D. M.; Kohlstedt, K. L.; Hersam, M. C.; Schatz, G. C.; Wasielewski, M. R.; Chen, L. X.; Facchetti, A.; Marks, T. J. Crystallography, Morphology, Electronic Structure, and Transport in Non-Fullerene/Non-Indacenodithienothiophene Polymer:Y6 Solar Cells. *J. Am. Chem. Soc.* **2020**, *142* (34), 14532–14547. https://doi.org/10.1021/jacs.0c05560.

(45) Natsuda, S.; Sakamoto, Y.; Takeyama, T.; Shirouchi, R.; Saito, T.; Tamai, Y.; Ohkita, H. Singlet and Triplet Excited-State Dynamics of a Nonfullerene Electron Acceptor Y6. *J. Phys. Chem. C* **2021**, *125* (38), 20806–20813. https://doi.org/10.1021/acs.jpcc.1c06448.

(46) Natsuda, S.; Saito, T.; Shirouchi, R.; Sakamoto, Y.; Takeyama, T.; Tamai, Y.; Ohkita, H. Cascaded Energy Landscape as a Key Driver for Slow yet Efficient Charge Separation with Small Energy Offset in Organic Solar Cells. *Energy Environ. Sci.* **2022**, *15* (4), 1545–1555. https://doi.org/10.1039/D1EE03565G.

(47) Neusser, D.; Sun, B.; Tan, W. L.; Thomsen, L.; Schultz, T.; Perdigón-Toro, L.; Koch, N.; Shoaee, S.; McNeill, C. R.; Neher, D.; Ludwigs, S. Spectroelectrochemically Determined Energy Levels of PM6:Y6 Blends and Their Relevance to Solar Cell Performance. *J. Mater. Chem. C* **2022**, *10* (32), 11565–11578. https://doi.org/10.1039/D2TC01918C.

(48) Moore, G. J.; Günther, F.; Yallum, K. M.; Causa', M.; Jungbluth, A.; Réhault, J.; Riede, M.; Ortmann, F.; Banerji, N. Direct Visualization of the Charge Transfer State Dynamics in Dilute-Donor Organic Photovoltaic Blends. *Nat. Commun.* **2024**, *15* (1), 9851. https://doi.org/10.1038/s41467-024-53694-4.

(49) Moore, G. J.; Causa', M.; Martinez Hardigree, J. F.; Karuthedath, S.; Ramirez, I.; Jungbluth, A.; Laquai, F.; Riede, M.; Banerji, N. Ultrafast Charge Dynamics in Dilute-Donor versus Highly Intermixed TAPC:C_{60} Organic Solar Cell Blends. *J. Phys. Chem. Lett.* **2020**, *11* (14), 5610–5617. https://doi.org/10.1021/acs.jpclett.0c01495.

(50) Zhong, Y.; Causa', M.; Moore, G. J.; Krauspe, P.; Xiao, B.; Günther, F.; Kublitski, J.; Shivhare, R.; Benduhn, J.; BarOr, E.; Mukherjee, S.; Yallum, K. M.; Réhault, J.; Mannsfeld, S. C. B.; Neher, D.; Richter, L. J.; DeLongchamp, D. M.; Ortmann, F.; Vandewal, K.; Zhou, E.; Banerji, N. Sub-Picosecond Charge-Transfer at near-Zero Driving Force in Polymer:Non-Fullerene Acceptor Blends and Bilayers. *Nat. Commun.* **2020**, *11* (1), 833. https://doi.org/10.1038/s41467-020-14549-w.

(51) Firdaus, Y.; Le Corre, V. M.; Karuthedath, S.; Liu, W.; Markina, A.; Huang, W.; Chattopadhyay, S.; Nahid, M. M.; Nugraha, M. I.; Lin, Y.; Seitkhan, A.; Basu, A.; Zhang, W.; McCulloch, I.; Ade, H.; Labram, J.; Laquai, F.; Andrienko, D.; Koster, L. J. A.; Anthopoulos, T. D. Long-Range Exciton Diffusion in Molecular Non-Fullerene Acceptors. *Nat. Commun.* **2020**, *11* (1), 5220. https://doi.org/10.1038/s41467-020-19029-9.

(52) Yang, W.; Pursglove De Castro, C. S.; Karuthedath, S.; Firdaus, Y.; Alshehri, N.; Chen, S.; Rosas Villalva, D.; Petoukhoff, C. E.; Dahman, A.; Baran, D.; Anthopoulos, T. D.; Laquai, F.; Gorenflot, J. Determining Exciton Diffusion Length in Organic Semiconductors: Unifying Macro- and Microscopic Perspectives. *Adv. Energy Mater.* **2025**, 2405322. https://doi.org/10.1002/aenm.202405322.

View Article Online
DOI: 10.1039/D6TA01925K

Data availability

The data that support the findings of this study are available from the corresponding author upon reasonable request. All relevant experimental data generated and analyzed during this study are included in the manuscript and its supplementary information.